Sensing and Bio-Sensing Research 38 (2022) 100511

Contents lists available at ScienceDirect

Sensing and Bio-Sensing Research

journal homepage: www.elsevier.com/locate/sbsr

Terahertz antenna based on graphene material for breast tumor detection☆

Radhoine Aloui [a,*], Hassen Zairi [a], Fermin Mira [b], Ignacio Llamas-Garro [b], Sofien Mhatli [c,d]

[a] Tunisia Research Laboratory Smart Electricity ICT, SEICT, LR18ES44, 45 Rue des Entrepreneurs 2035, National Engineering School of Carthage, University of Carthage, Tunisia
[b] Centre Tenologic de Telecommunication de catalunya (CTTC/CERCA), 08860 Castelldefels, Spain
[c] SERCOM-Lab, EPT Université de Carthage, La Marsa, Tunis 2078, Tunisia
[d] ISI KEF, 5 rue saleh Ayech, kef 7100, Université de Jendouba, Tunisia

ARTICLE INFO

Keywords:
Terahertz band
SIW technology
PBG
Biosensor
Breast tumor detection
Graphene material
Chemical potential

ABSTRACT

In this paper, two different types of graphene-based rectangular patch antennas are designed for broadband terahertz applications. First, a patch antenna is modeled using copper metal for terahertz applications. The simulation results show a degraded reflection coefficient due to the use of copper. Therefore, the reflection coefficient is above -10 dB at 4.6 THz, then a VSWR is less than 3 dB when we used copper for the top patch. The patch antenna results are improved when graphene material is used, which has good conductivity, as demonstrated through simulations. Furthermore, an increasing band-width of 1 THz instead to 0.8 THz when we used the graphene material, due to a better impedance match. On the other hand, we achieved a slight increase in gain and the VSWR is less than 2 dB inside the available bandwidth.

The time-domain solver of CST MWS software is used to evaluate the performance of the SIW (Substrate Integrated Waveguide) patch antennas. The SIW, PBG technology and the graphene material makes the antenna very important due to performance, such as the gain increases to about 7 dB, the bandwidth is about 1.6 THz duo to increase the chemical potential of the graphene material. The results obtained with CST are compared with simulations using HFSS to validate the design further. In addition, the 10 g peak skin SAR values of the antenna are 1.726e7 W/Kg instead of 9.55e5 W/Kg. In these results we conclude the antenna can detect tumor presence.

1. Introduction

The terahertz band is the electromagnetic spectrum portion, with frequencies in the range from 0.3 THz to 20 THz [1]. Optical spectrum systems have received considerable interest from the scientific community for terahertz (THz) generation and imagery, with numerous spectroscopy applications, imaging, sensing, astronomy, spectroscopy, etc. [2–8]. Terahertz communication and imaging domains have recently increased in optoelectronic systems, although cutting-edge technology for payload systems and medical imaging must still develop. Researchers had become attracted to new technology during previous years, called substrate integrated waveguide technology. This technology has a good performance for many applications, in particular for terahertz domains [9]. Several circuits are found among these circuits, such as: antenna, resonator, coupler, duplexer and power divider [10]. The substrate integrated waveguide structure needs significant memory storage and an important calculation time when dealing with terahertz domain designs. However, there are only a few Terahertz antennas which can be realized with wideband characteristics simultaneously with a high gain for imagery applications and Terahertz telecommunications. The scientific community constantly uses optical spectrum systems for generation and imagery using terahertz (THz) radiation, with numerous spectroscopy applications, imaging, sensing, astronomy, and spectroscopy [11,12]. In order to obtain a high-performance circuit, copper can be replaced for graphene, resulting in improved terahertz circuits. The discovery of graphene is a breakthrough in the development of THz devices and applications [13]. Terahertz devices [14] have been crucial and attractive for research activities during recent years, due to the limited and congested GHz band. The discovery of graphene material is a breakthrough impacting the development of THz devices and applications. A graphene-based receptor with outstanding flexibility and compactor properties has

☆ Fully documented templates are available in the elsarticle package on CTAN.

* Corresponding author.
E-mail addresses: Radhoine.aloui1990@gmail.com (R. Aloui), hassen.zairi@gmail.com (H. Zairi), fermin.mira@cttc.cat (F. Mira), ignacio.llamas@cttc.es (I. Llamas-Garro), sofienmhatli2017@gmail.com (S. Mhatli).

https://doi.org/10.1016/j.sbsr.2022.100511
Received 26 April 2022; Received in revised form 11 July 2022; Accepted 1 August 2022
Available online 8 August 2022

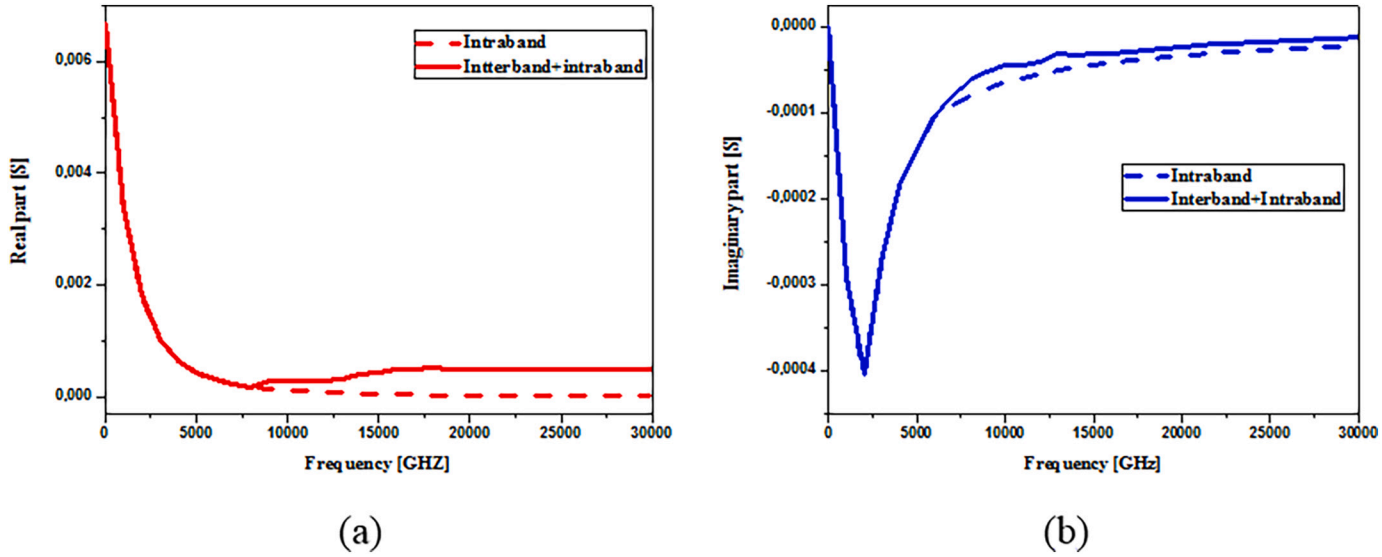

Fig. 1. Comparison of the total and intraband conductivity of the graphene sheet: (a) Real part, and (b) imaginary part.

been presented in [13]. To avoid congestion, it is attractive to find a wideband and high gain antenna, compatible with many terahertz system devices and applications. In this paper, a new wideband antenna working in the terahertz band with a simple layer and microstrip feed line is presented. The proposed antenna is developed using SIW technology with a PBG structure. The proposed wideband antennas are illustrated in Fig. 5, including their geometry. However, the proposed antenna is used for THz band to make a biosensor for breast Tumor detection. The paper is organized as follows, section 2 describes the formalization of the graphene material and the antenna parameter design such as resonance frequency and structure, including the PBG equation. Section 3 presents the antenna design the first results about the comparison between the two material (copper vs graphene) and the effect of integrated SIW technology insie the substrate is describe in this section. Section 4 is describes the comparasion between antennas validated using two simulators (CST and HFSS). The detection of the breast tumor is shown in section 5. Fincally, the conclusion is proved in section 6. (See Fig. 1.)

2. Formulation

2.1. Graphene conductivity

The graphene sheet is a two-dimensional material composed of carbon atoms bonded in hexagonal structures. Its surface conductivity can be represented using the well-known Kubo formalism and it consists of two terms, intraband conductivity and interband conductivity [15,16]. The intraband term can be calculated as

$$\sigma_{intra} = -j\frac{e^2 K_B T}{\pi\hbar^2(\omega - j2\Gamma)}\left[\frac{\mu_c}{K_B T} + 2ln\left(e^{-\frac{\mu_c}{K_B T}} + 1\right)\right] \quad (1)$$

and the interband conductivity is

$$\sigma_{inter} \simeq -j\frac{e^2}{4\pi\hbar}ln\left[\frac{2|\mu_c| - (\omega - j2\Gamma)\hbar}{2|\mu_c| + (\omega - j2\Gamma)\hbar}\right] \quad (2)$$

Where K_B is the Boltzmann constant, $\hbar$ is the reduced Planck's constant, e is the electron charge, ω is the angular frequency, Γ is the scattering rate, T is the temperature and μ_c is the chemical potential. The intraband conductivity dominates the value of total conductivity in the

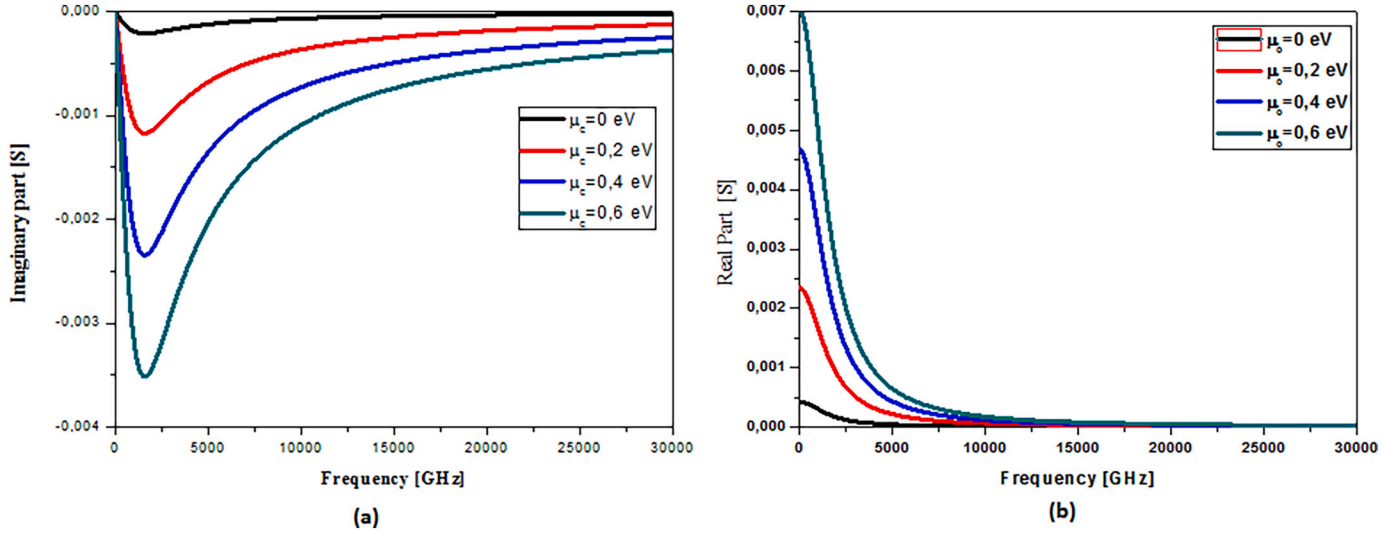

Fig. 2. Variation of the total conductivity for different chemical potentials: (a) Real part and (b) imaginary part.

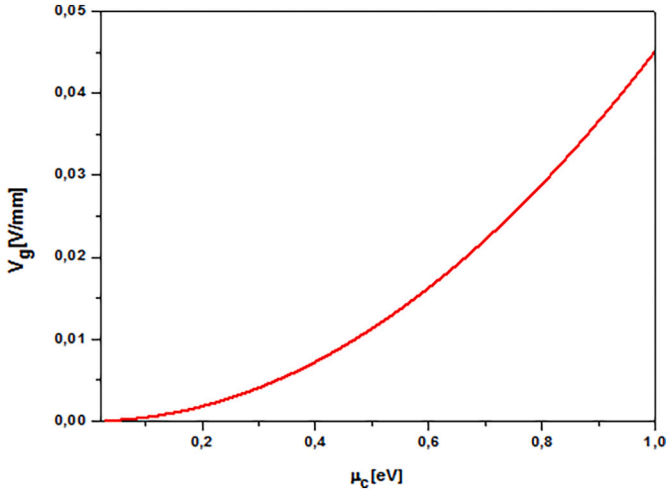

Fig. 3. The relationship between bias voltage and chemical potential.

THz band, whereas the interband term has no significant effect on the total surface conductivity within this band. Hence, the conductivity of graphene can be expressed by using only theintraband term.

According to eqs. (1,2), the graphene material can be shown in two types of domains. In the first step, the intraband is dominant in the frequency range from 0 to 8 THz. Elsewhere, in the frequency range from 8 to 30 THz of the interband and intraband [8,9] should be considered.

Fig. 2 shows the effect of changing graphene chemical potential on the real and imaginary parts of the surface conductivity. It depends on the carrier density, which can be controlled by an electric bias field. Furthermore, we present in Fig. 3 the relation between the bias voltage and chemical potential in the graphene material from Eq. (3).

$$V_g = \frac{e\mu_c^2}{\pi h V_g \varepsilon_0 \varepsilon_r} \tag{3}$$

We conclude that the chemical potential increases consequential to bias voltage growth, hence the increase of the conductivity can be shown in Fig. 3. The resonance frequency shift is due to change.

2.2. Analysis of SIW cavity rectangular antenna

In this part, the procedure calculates the width and length of a SIW cavity, for the TEmn resonant frequency mode. According to Eq. (4), the resonant frequency of the SIW cavity is fixed by setting the cavity length and width simultaneously.

$$f_{mn} = \frac{1}{2\sqrt{\mu_r \varepsilon_{reff}}} \sqrt{\left(\frac{m}{L}\right)^2 + \left(\frac{n}{W}\right)^2} \quad ; \varepsilon_{reff} \le \frac{1+\varepsilon_r}{2} \tag{4}$$

where L and W are the length and the width of the proposed patch antenna, respectively.

$$Z_{in} = \frac{1 - S_{11}}{1 + S_{11}} \tag{5}$$

Where S_{11} is calculated by

$$S_{11} = \frac{\Gamma_0 (1 - e^{j2nK_0 e})}{(1 - \Gamma_0^2 e^{j2nK_0 e})} \tag{6}$$

Where, e is the maximum dimension of the dielectric, m is the periodicity branch of the cosine function, the refractive index n is calculated using [17] and K_0 is the wavenumber in the void. The refractive index can have two parts, the real component and the imaginary part. The permittivity and permeability can be calculated using the following expression, respectively:

$$\varepsilon = \frac{n}{Z_{in}} \quad and \quad \mu = nZ_{in} \tag{7}$$

2.3. Mathematical expression analysis of the PBG structure

A PBG structure is embedded in the proposed antenna design. Fig. 4 shows the 2D and 3D structure of the dielectric material with the substrate's hollow cylindrical structures. It can be seen from Eq. (8) that the structure at the substrate level is useful for the propagation of the EM waves. The mathematical expressions for plane wave propagation along the PBG substrate are as follows: For TM modes:

$$\frac{\partial^2 E_Z}{\partial x^2} + \frac{\partial^2 E_Z}{\partial y^2} + K^2 n^2 E_Z = 0 \tag{8}$$

For TE modes:

$$\frac{-2}{n^3}\left(\frac{\partial n}{\partial x} + \frac{\partial n}{\partial y}\right) + \frac{1}{n^2}\left(\frac{\partial^2 H_Z}{\partial x^2} + \frac{\partial^2 H_Z}{\partial y^2}\right) + K^2 H_Z = 0 \tag{9}$$

where n is the plane wave refraction, dependent to (x,y) and k is the wavenumber k = $2\pi / \lambda$. Fig. 4.a shows the square lattice structure, with circular cross-section holes, resulting in a cylindrical dielectric column with radius 'r', and a period of 'd' which lies on the x-y plane. Fig. 4.b shows the PBG dielectric substrate with the cylindrical holes with radius 'r' and the same separation distance of 'd'.

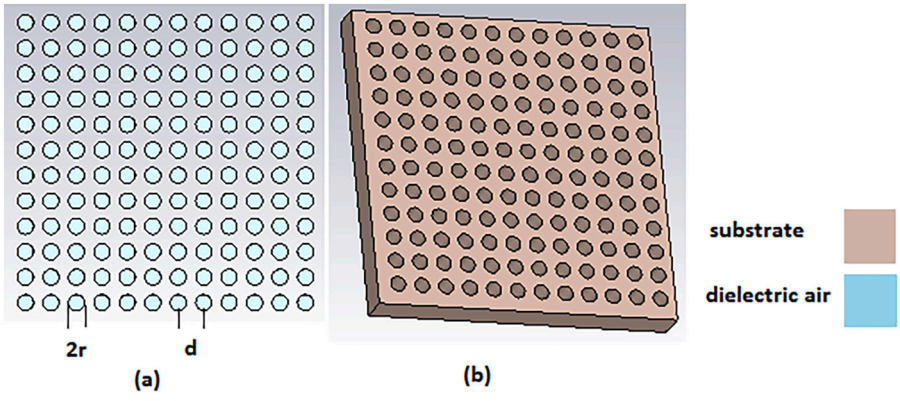

Fig. 4. PBG structure (a) Dielectric column in air (b) cylindrical hole structure on the substrate.

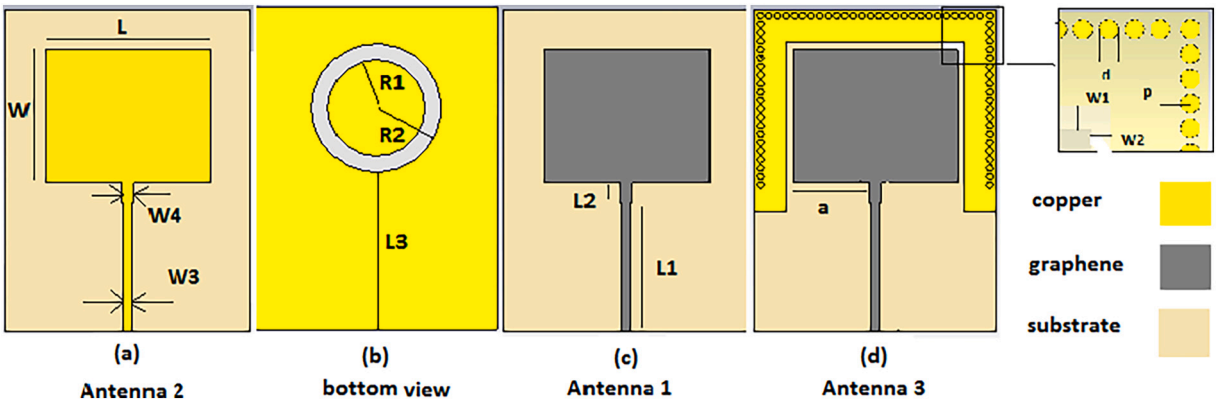

Fig. 5. Proposed antennas; (a) Top view Antenna 1; (c) Top view Antenna 2; (d) Top view Antenna 3(with SIW cavity).

Table 1
Antenna design parameters.

Parameter	*L*	*W*	*R*1	*R*2	*L*1	*L*2	*L*3	*W*1	*W*2	*W*3	*W*4	*h*	*d*	*p*
Value [*um*]	33	21	12	16	32	5	39	2	1.5	2	3	2	0.6	1.1

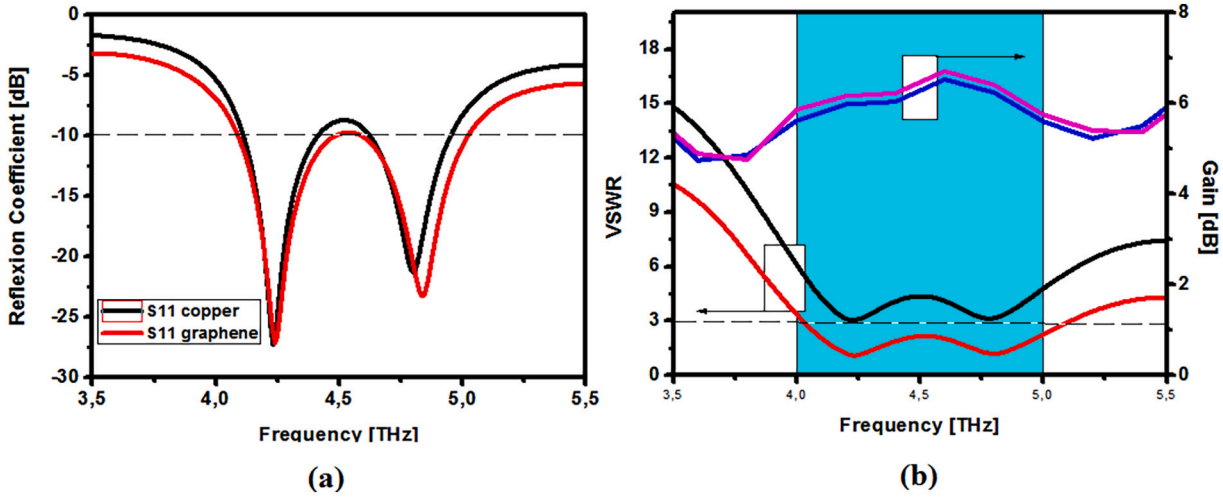

Fig. 6. (a) Reflections coefficients of the two materialstypes of antenna; (b) VSWR and gain versus frequency of proposed antennas.

3. Proposed antennas designs and comparison of antennas results

The proposed antennas designed are illustrated in Fig. 5. The front view is shown in Fig. 5.a, c and d, corresponding to antenna 2, 1 and 3 respectively, with the same bottom view for all, shown in Fig. b. Table 1 gives the optimized dimensional parameters of the proposed antennas.

In the first step, the proposed antenna is simulated and studied using the CST simulator based on an integral method. According to Fig. 6.a and Fig. 6.b, the simulation results for antennas (1, 2) are shown providing a comparison between the two materials used, copper and graphene, where improvement is obtained when the graphene material used. Moreover, secondly, SIW technology has been used for improving the outer antenna performance. The PBG structure's impact at the substrate level is illustrated in Fig. 4 for the proposed SIW antenna, used to improve antenna performance.

3.1. Comparison between two material

In this paper, to improve the proposed antenna design to work in the terahertz domain, graphene material is used to form the top patch instead of copper in the first step, according to Fig. 5.a and Fig. 5.c. A comparison of the s-parameters results, VSWR and gain of antenna, is illustrated in Fig. 6. Copper conductivity suffers at terahertz region thats why we use gold and other plasmonic material though graphene is best at terahertz region offer ring tunable performance when change in chemical potential. However it require complex fabrication procedure and also the conductivity changes with incresing graphene thickness [18].

According to Fig. 6.a which shows a reflection coefficient S11 of the patch antenna, the S11 level improvement is obtained when using graphene material instead of copper. Moreover, from this result, S11 can be below a -10 dB when using graphene material to form the top patch. Graphene shows good conductivity and high performance at terahertz frequencies.

Fig. 6.b shows the simulated curve gains, which are about 5 dB and 7 dB when using graphene material to form the top patch. On the other hand, 4.5 dB and 6.6 dB are obtained when copper is used to form the top patch. However, in the same figure, the values obtained for voltage standing wave ratio (VSWR) when using the two materials, graphene

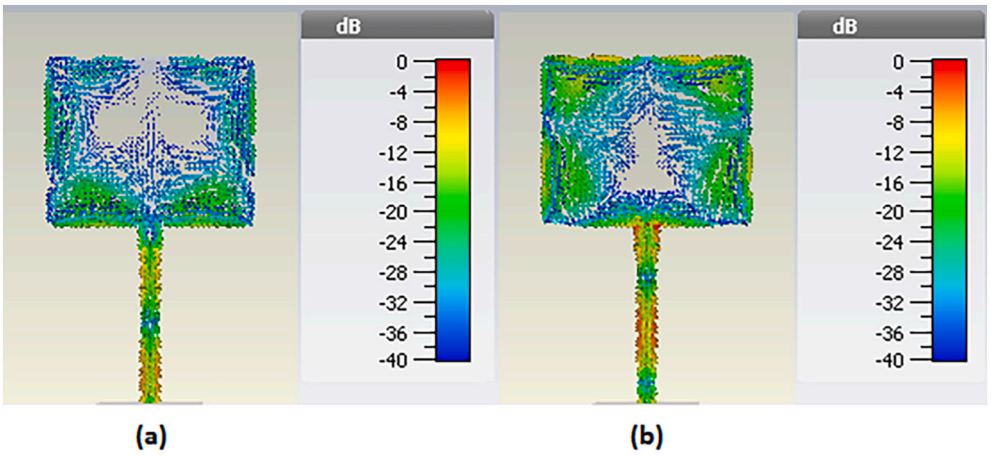

Fig. 7. Current distribution (a) Copper (Antenna2) (b) Graphene (Antenna1).

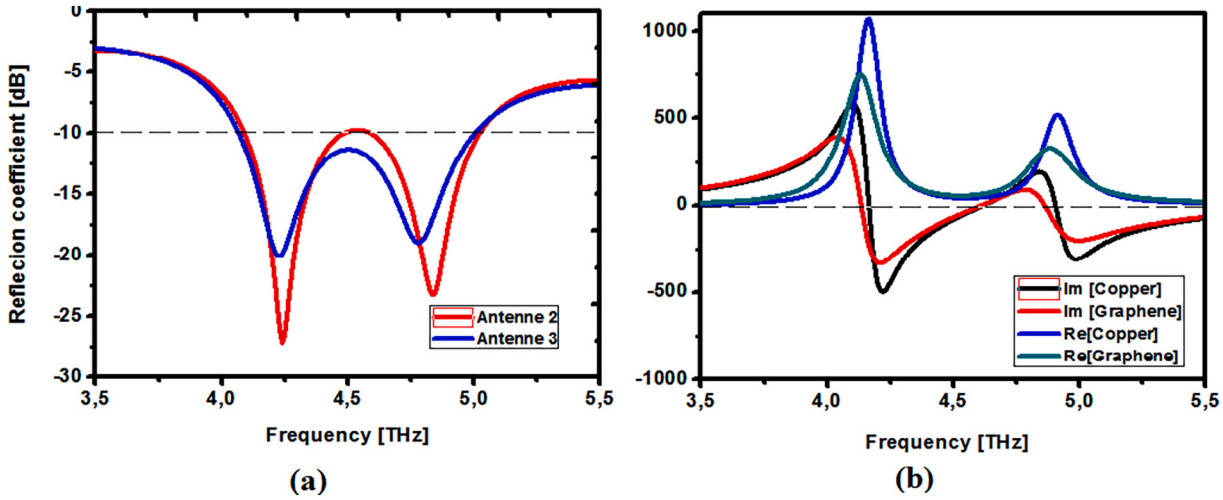

Fig. 8. (a) Reflections coefficients of the proposed antenna with and without SIW cavity; (b)Input impedance characteristic of the proppsed antennas 1,3 (Imaginary and Real) with respect to frequency.

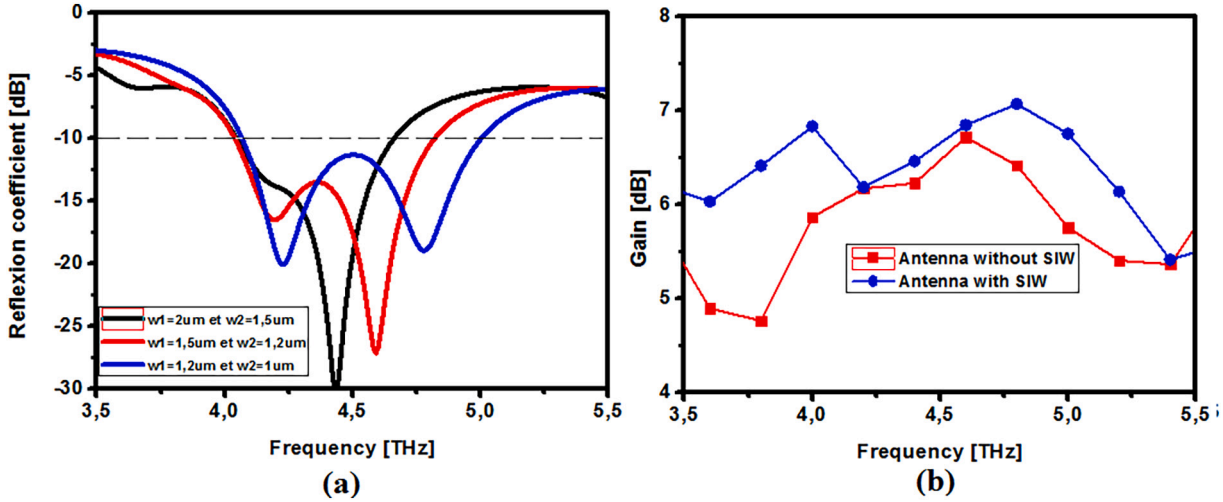

Fig. 9. (a) Reflection coefficient frequency plot by changing the SIW cavity dimension; (b) Effect on reflection coefficient by changing the chemical potential.

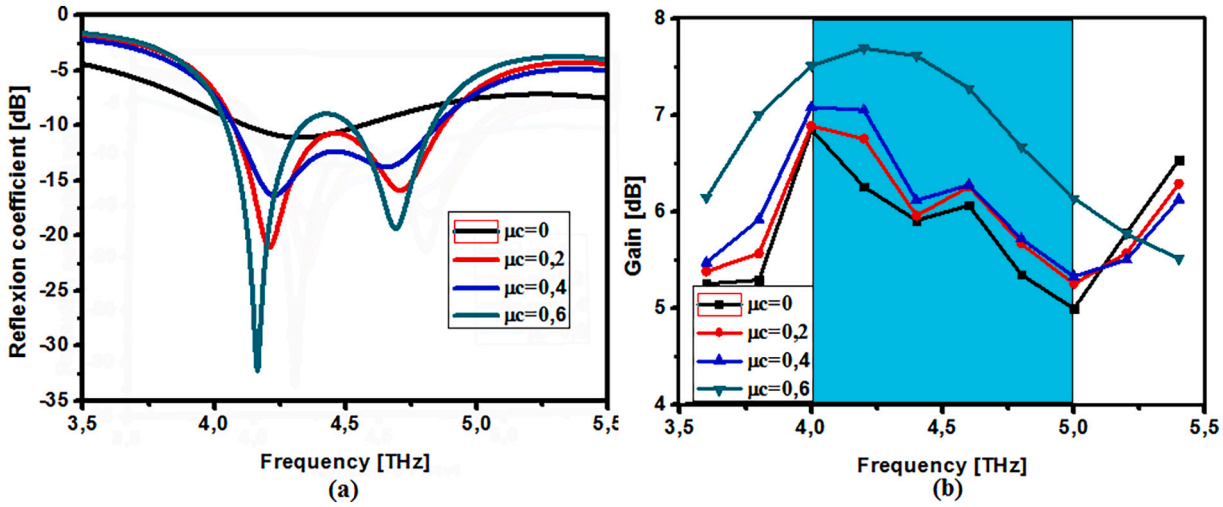

Fig. 10. (a) Effect on reflection coefficient by changing the chemical potential including interband and intraband (b) Effect on Gain by changing the chemical potential with two conductivity domains.

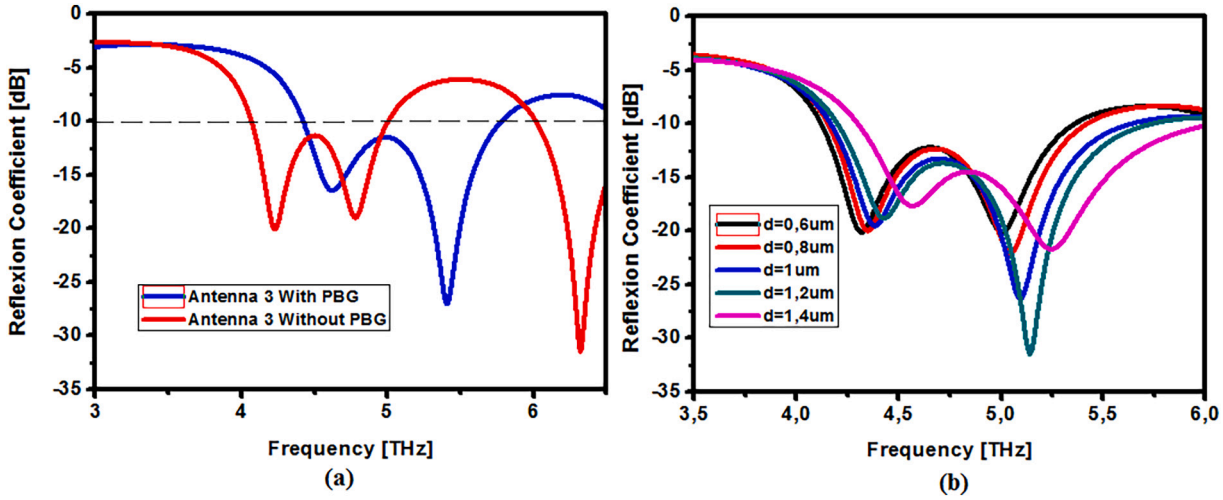

Fig. 11. (a) Reflection coefficient with PBG and without PBG of the proposed antenna; (b) Reflection coefficient with versus radius of PBG.

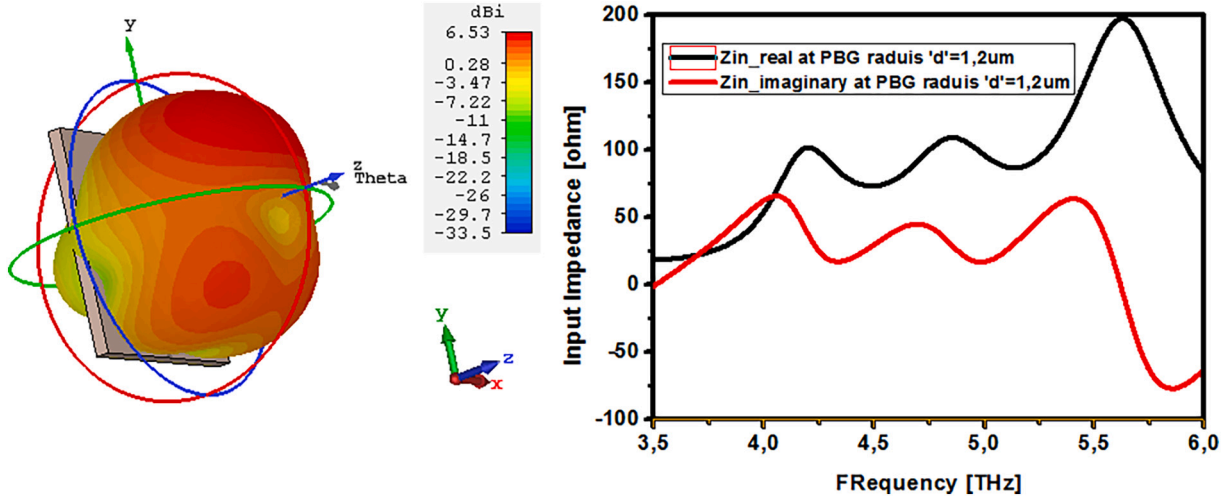

Fig. 12. (a) Simulated 3-D radiation pattern (b)Input impedance behavior with frequency.

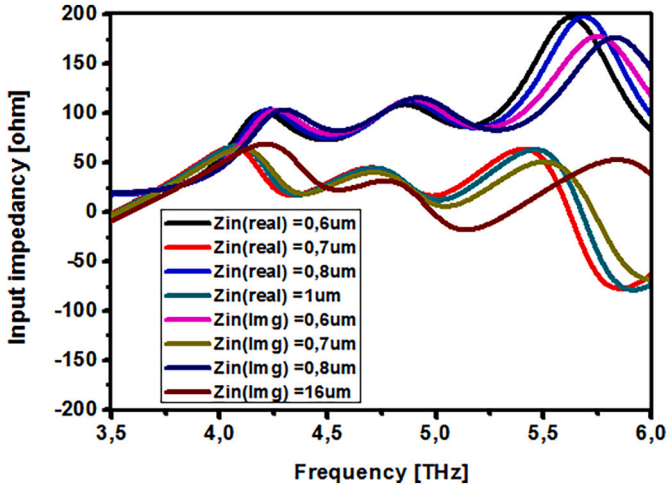

Fig. 13. Input impedance versus radius of PBG.

and copper is shown. VSWR then can be less to 3 dB when graphene material is used. Graphene material shows a good result, including improved current density distribution in the top patch, as illustrated in Fig. 7.

3.2. Analysis for SIW cavity technology

In order to improve the reflection coefficient S11 of the proposed antenna, the technology shown in Fig. 5.d is used, consisting of applying the SIW technology to form the outer part of the antenna. The simulation S-Parameters results can be shown in Fig. 8.a. According to this figure, an improvement in the reflection coefficient level is obtained, below the reflection coefficient of antenna2, when using the SIW technology to form the outer part of the antenna, as illustrated in Fig. 8a. This improvement is due to the uniform current density in the top patch antenna by introducing the SIW cavity. Fig. 8.b shows a proper impedance match for the input feed line for both graphene and copper material used to form the top patch. After optimizing the antenna using the CST software, the right impedance and radiation performance can be achieved with parameters fixed, such as those considered for the initial parameters. Fig. 9.a shows the reflection coefficient obtained when varying w_1 and w_2 according to the substrate integrated waveguide cavity in Fig. 5.d. However, The SIW cavity increases antenna gain, from 6 dB at 4 THz without the SIW cavity to 7 dB at 4 THz with SIW cavity.

However, Fig. 9.b shows the rise of gain when we add the SIW technology. It can make the gain above 7 dB when we add the SIW structure in the outer antenna substrate. To explore the usefulness of graphene's tunable surface conductivity in microwave antenna design, simulated reflection coefficients (S11) of the SIW proposed antenna with $w_1 = 1.2\ \mu_m$ and $w_2 = 1\ \mu_m$, is presented in Fig. 10.a. An improvement in the reflection coefficient is obtained when increasing the chemical potential. Finally, the proposed antenna gain can be increased by increasing the chemical potential of graphene, as presented in Fig. 10.b.

3.3. Analysis of the PBG and tuning frequency

In this part we compare two antennas (Antenna3) and on the other hand we add a PBG structure at the substrate level. The antennas design in Fig. 5 (d) with PBG structure can be made to work at terahertz frequencies. Fig. 11 (a) shows the reflection coefficient canbe optimized to be below -10db and with 1.4 THz bande when using the PBG structure. The PBG technology can increase the bandwidth to 33.4% instead 23.84 % without PBG. Moreover, to improve these results, we adjust the radius value of the PBG structure, the simulation results show an improvement in reflection coefficient and we have a good matching input impedance when the radius value increases, we notice the return loss is below −15 dB, then an increasing antenna bandwidth is presented in Fig. 11.b. Fig. 12.a illustrates the three dimensions radiation pattern of the proposed PBG antenna at 4.2 THz frequency. Clearly demonstrating a unidirectional antenna. Then, an important notice, the improvement on simulation gain is due when increasing of the PBG radius. The variation of input impedance (real and imaginary) with frequency is displayed in Fig. 12.b. The well-matched real value of impedance is found 50 at 4.2 THz and chemical potential of 0.6 eV. Moreover, with radius decreasing, the impedance Z_{input} gets better. The variation of input impedance (Real and Imaginary) versus frequency is plot in Fig. 13. The well-matched real value of impedance is found to be 50 *ohm* at 4.2 THz and PBG radius of 0.8 μm.

3.4. Behavior of the doped graphene-based patch antennas

This section, we perform a detailed discussion of the performance antenna with graphene instead of copper material. Table 2 illustrates the results antenna by changing the chemical potential value of graphene. Therefore we have changed the parameter of the SIW technology (W1, W2) is modeled in this section. Since, we are modeling three models of graphene antennas compared with the copper patch material. G1, G2 and G3 are referred to as 0 eV, 0.2 eV and 0.6 eV of chemical potential value, respectively. Table 2 shows the comparison between the three models antenna (G1, G2 and G3), their performance is focus in terms resonance frequency (f_r), reflection coefficient, Bandwidth, Directivity, angular width at -3 dB and Gain are summarized in this table.

According to this table, we have an improvement of the antenna performance when we use the graphene material in the first step. On the

Table 2
Performance comparaison of the proposed antenna without and with SIW technology vs chemical potential, undoped and doped graphene.

d = 0.6um, p = 1.1um, L = 33um, w = 21um, h = 2um and the dielectric of the substrate is Duroid = 2.2

G1 = Doped graphene with 0.2 eV, G2 = Doped graphene with 0.4 eV and G3 = Doped graphene with 0.6 eV

Parameter of graphene	Conducter material	*fr* in THz	*S11 at fr* in -dB	BW at −10 dB in THz	*Directivity* at fr in dB	Angular width at −3 dB [deg]	Gain in dB
4*W1 = 2um and W2 = 1.5um	copper	4.25	20	0.5	6.5	50	6
	G1	4.29	27.2	0.55	6.68	51.2	6.3
	G2	4.22	28.1	0.647	6.8	51	6.35
	G3	4.14	29	0.7	6.82	49	6.4
4*W1 = 1.5um and W2 = 1.2 um	copper	4.36	21.3	0.6	6.6	47	6.2
	G1	4.45	28	0.87	7	49	6.31
	G2	4.31	31.5	0.9	7.2	47.6	6.5
	G3	4.23	32.8	0.94	7.23	47	7
4*W1 = 1.2um and W2 = 1um	copper	4.6	22	0.67	6.4	47	6.12
	G1	4.75	30	0.9	7.48	48.3	6.45
	G2	4.71	33.9	0.97	7.5	48.1	6.8
	G3	4.67	34	1.02	7.56	48	6.89

Table 3
Performance comparison of the proposed antenna for various substrate materials.

Substrate parameter	Chimical potential [eV]	Reso. Freq. [THz]	Return Loss [dB]	Bandwidth [THz] < −10	VSWR [dB]	Gain [dB]
ptPolymide $\varepsilon_r = 3.5$	$\mu_c = 0.4$	4.15	−32.5	1.5	1.25	7.5
	$\mu_c = 0.3$	4.25	−21.3	1.35	1.255	6.88
	$\mu_c = 0.2$	4.28	−15	1.3	1.3	6.02
	$\mu_c = 0.1$	4.31	−11	0.9	1.34	6
ptArlon $\varepsilon_r = 3$	$\mu_c = 0.4$	4.45	−31.25	1.47	1.3	7
	$\mu_c = 0.3$	4.49	−20.08	1.25	1.45	5.78
	$\mu_c = 0.2$	4.58	−12.5	1.2	1.57	5.67
	$\mu_c = 0.1$	4.66	−10.2	0.89	1.7	5.45
ptDuroid $\varepsilon_r = 2.2$	$\mu_c = 0.4$	4.54	−29.87	1.4	1.32	7.2
	$\mu_c = 0.3$	4.6	−20.54	1.21	1.8	5.49
	$\mu_c = 0.2$	4.71	−12.3	0.98	2	5.4
	$\mu_c = 0.1$	4.78	−10	–	2	5.45

other hand the chemical potential can be tuned the resonance frequency such as: An increase for the μ_c can decrease the fr (4.29 to 4.14) when G1 is used, also an improvement in the gain (6.3 to 6.4 dB). It is also a slight improvement in bandwidth (0.55 to 0.7 THz) and finally the reflection coefficient it can be decreasing at −32,8 dB. In the same context an increase of the chemical potential makes: decrease fr 4.45 to 4.23 THz, increase the gain and directivity of the antenna.

Another parametric study at the dielectric level, since for various substrate materials, the resonant frequency shift is observed of the 4.15–4.54 THz when the dielectric permitivity is decreasing. The bandwidth achieved is in the range 0.9–1.47 THz at different resonance frequencies as depicted in Table 3. It can be seen that the maximum bandwidth of 1.47 THz is obtained for the Arlon substrate with $\mu_c = 0.4$ eV.

4. Comparison between the antennas and validated results

4.1. Comparison between the antennas

Performance radiation of the proposed antennas 1, 2, 3 and 4 (see Fig. 5) has been compared and analyzed. CST microwave studio based on the FDTD method simulates the antennas results radiation and S-parameters at the frequency range [3.5–6 THz].

Fig. 14.a shows the reflection coefficient plot for the proposed antennas. The bandwidth obtained for the proposed antennas are below −10 dB, except for Antenna 1 when using a simple material (Copper) due to its low conductivity. The return loss simulation results are almost equal to −10 dB at the [4.5–5 THz] band with antenna 2. Improved results are obtained with antennas 3 and 4 when the SIW cavity in the outer antenna and the PBG structure are added.

In the same Fig. 14.b, the E plane plot at 4.2 THz is investigated corresponding to the four antennas. The obtained far-field polar plot in Fig. 13.b shows that the maximum radiation is 45^0 for antenna 1, 2, 3 and 4, respectively.

According to Fig. 14 (b), an improvement is obtained for the radiation pattern at 4.2 THz, when the SIW cavity and the PBG structure at the substrate level are added. Moreover, the achieved angular widths are 40^0 to 46^0 for antenna 1 and 2 respectively. Then 116.3^0 to 121.5^0 for antenna 3 and 4, respectively.

4.2. Validated results and discussion

In this part, the validation of the designed SIW antenna is done by simulating the same antennas with the HFSS software (FEM) and comparing the results with those obtained with CST (FDTD). Figs. 15 and 16 provide the simulation results in terms of reflection coefficient and radiation pattern (E-plane and H-plane).

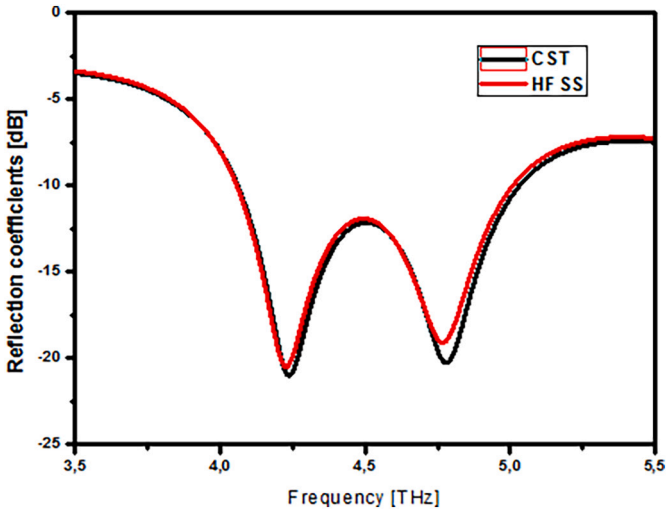

Fig. 15. Reflection coefficient of the propsed antenna, simulated using CST and HFSS.

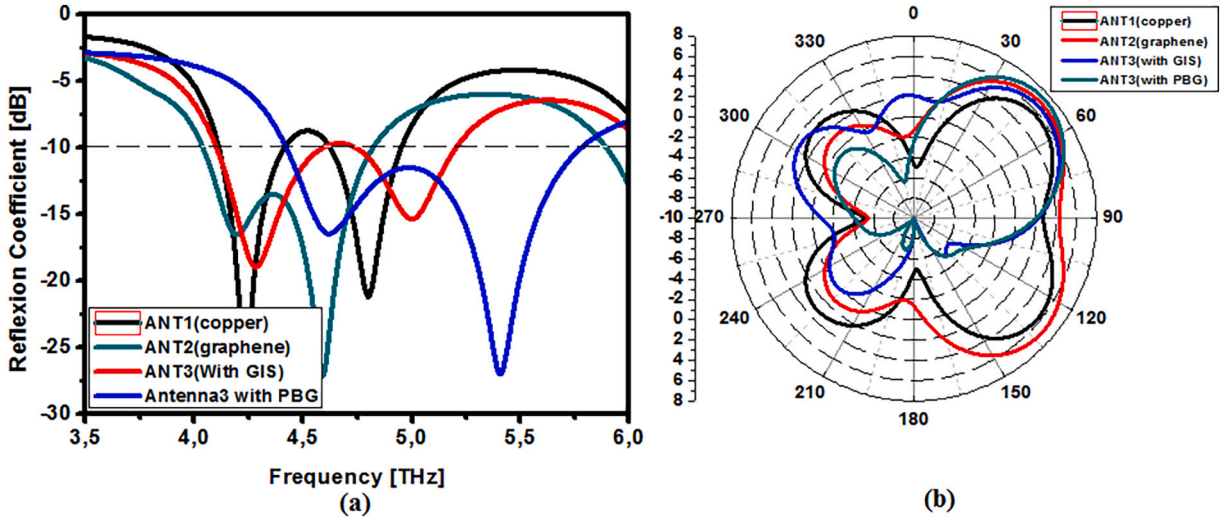

Fig. 14. (a) Reflection coefficient, (b) Radiation pattern (*E*-plane at 4.2 THz.

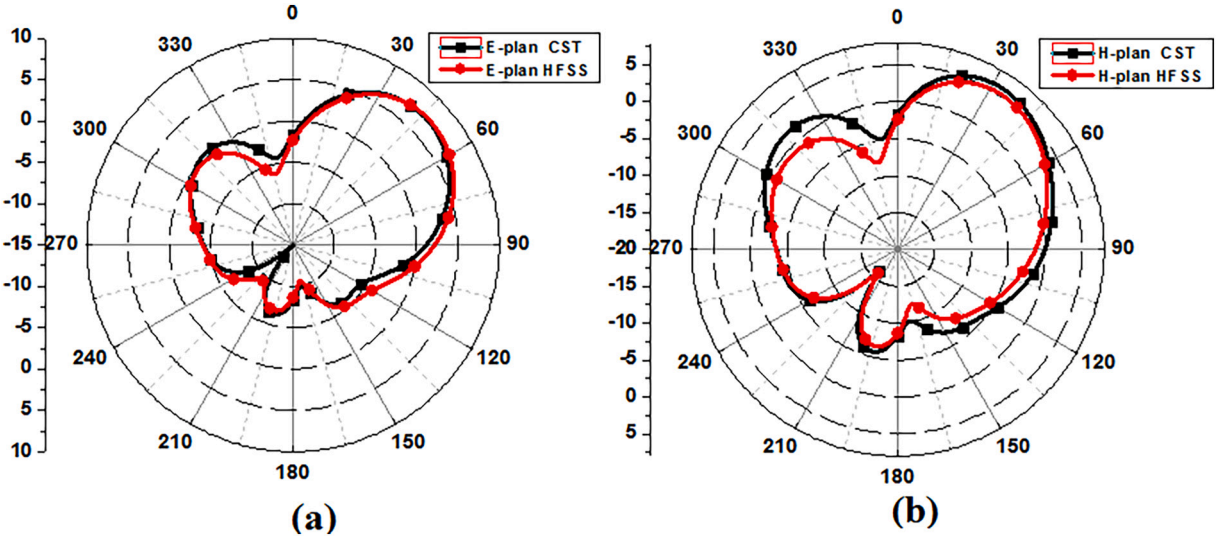

Fig. 16. Radiation pattern of the proposed antenna, simulated using CST and HFSS: (a) E-plane at 4.2THz. (b) H-plane at 4.2 THz.

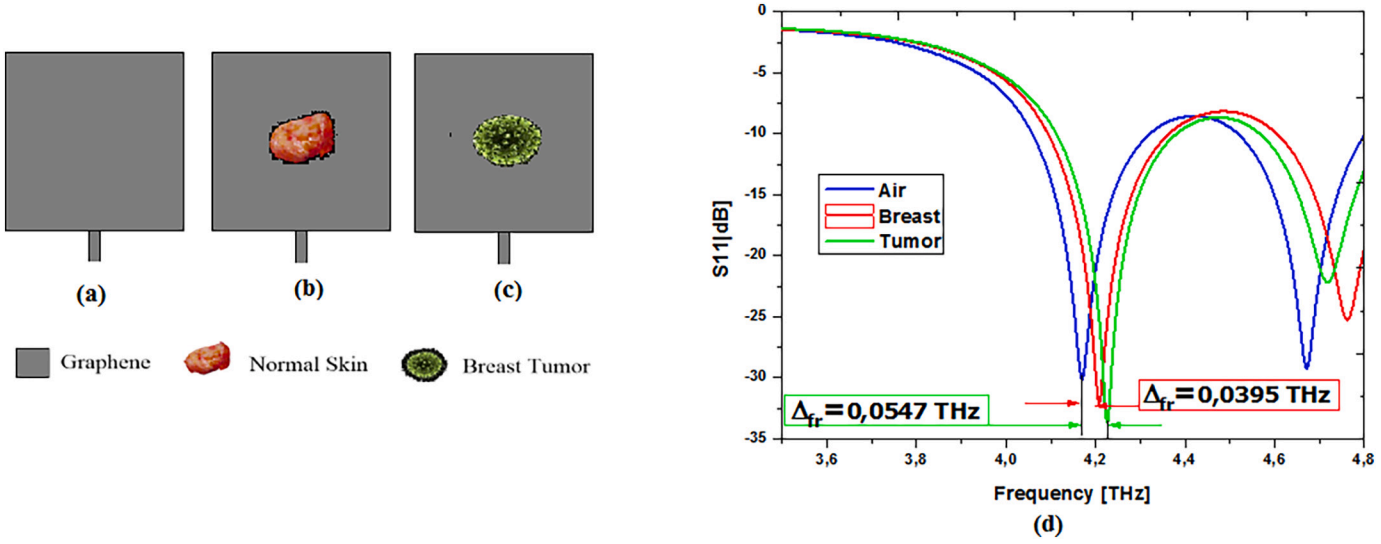

Fig. 17. Schematic representation of the proposed sensor structure: (a) antenna with Graphene material, (b) loaded with a normal human breast tissue, (c) loaded with breast tumor tissue, and (d) Simulation results of the graphene-based sensor for different material under test.

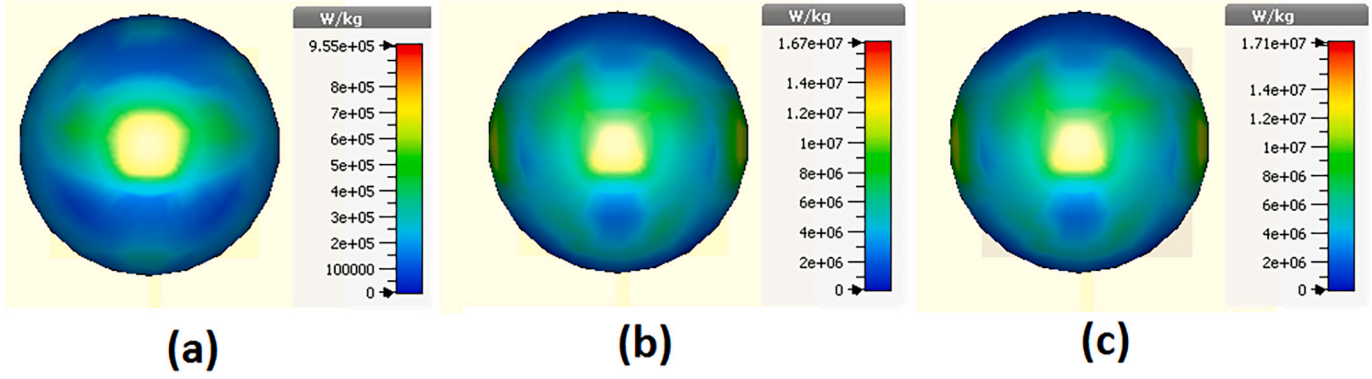

Fig. 18. SAR Distributions at 4.25 THz; (a) antenna with normal Skin, (b) antenna with Tumor (copper material) and (c) antenna with tumor (graphene instead copper).

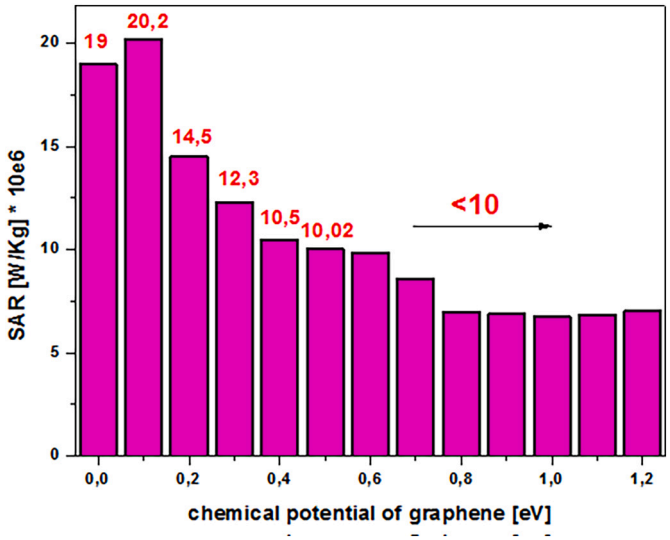

Fig. 19. SAR with versus of the chemical potential of graphene.

Table 4
Comparisons between referred antennas and proposed antennas.

References	Sensitivity(THz/RIU)	FOM (RIU-1)	f_{res}[THz]
[23]	2	10.5	0.91
[24]	0.22	1.1	0.71
[25]	1.9	6.56	11.5
This work	7.26	19.78	4.25

According to Fig. 15, a good agreement in S11 is observed when comparing the CST and HFSS. A slight deviation in the side-lobe level is found. As shown in Fig. 16, a good agreement is observed for E-plane and H-plane gain radiation patterns vertically, from Fig. 15 at 4.2 THz frequency.

The proposed antennas simulation has a maximum gain of 7.6 dB and can vary as much as 5 dB between the 4 and 5.5 THz frequency range.

5. Breast tumor detection and sensing

To analyze the sensing parameters of the proposed sensor, the proposed antenna is fixed near breast tissues cells (normal and tumor breast tissues). To test the cells, we must compare two type of cells, one with tumor and the other one without tumor. The effect of the variation of these biological cells change the resonance frequency shift of the antenna as shown in Fig. 17. Therefore, we conclude the proposed sensor has a resonance frequency shift when we change the cells with and without tumor towards the high frequencies. In biosensors, the sensitivity (s), figure of merit (FOM), and quality-factor are the important parameters that show the sensing quality, defined as described in [19,20].

The specific absorption rate (SAR), is based on the IEEE C95.1 standard, this last is determined here using the mass average method calculated using CST software. As presented in Fig. 18, the cell skin or tumor for cell (Breast) developed by CST is exploited for testing. The separation between the proposed graphene antenna and the cell is set at 20 um. Furthermore, in Fig. 15 it can be seen that maximum SAR of the breast/Tumor when the graphene is used instead of copper, at 1-mg of tissues are below the existing regulations [21–25] in all the cases. The SAR results can be calculated by [26], according to the Fig. 18 it can be shown the 1-mg peak SAR value is 1.71e+7 W/Kg with maximum allowable powers of the proposed antenna are 0.07 W at 4.25 THz.

$$sensitivity = \frac{\Delta f}{\Delta n}(THz/RIU) \tag{10}$$

$$Figure\ of\ Merits = \frac{f_{res}}{Full - WidthatHalf - Maximum}\left(RIU^{-1}\right) \tag{11}$$

$$Quality - factor = \frac{sensitivity}{Full - WidthatHalf - Maximum}\left(RIU^{-1}\right) \tag{12}$$

(See Fig. 19.)

Where Δn et Δf are the refractive index and resonance frequency respectively. Where ($\Delta n = n_{Air} - n_{(Normal\ Breast/Tumor\ Breast)}$) and ($\Delta f = f_{Air} - f_{(Normal\ Breast/Tumor\ Breast)}$).

The sensing parameters of this graphene proposed antenna sensor are compared with other works, and reported in Table 4. In this table, we

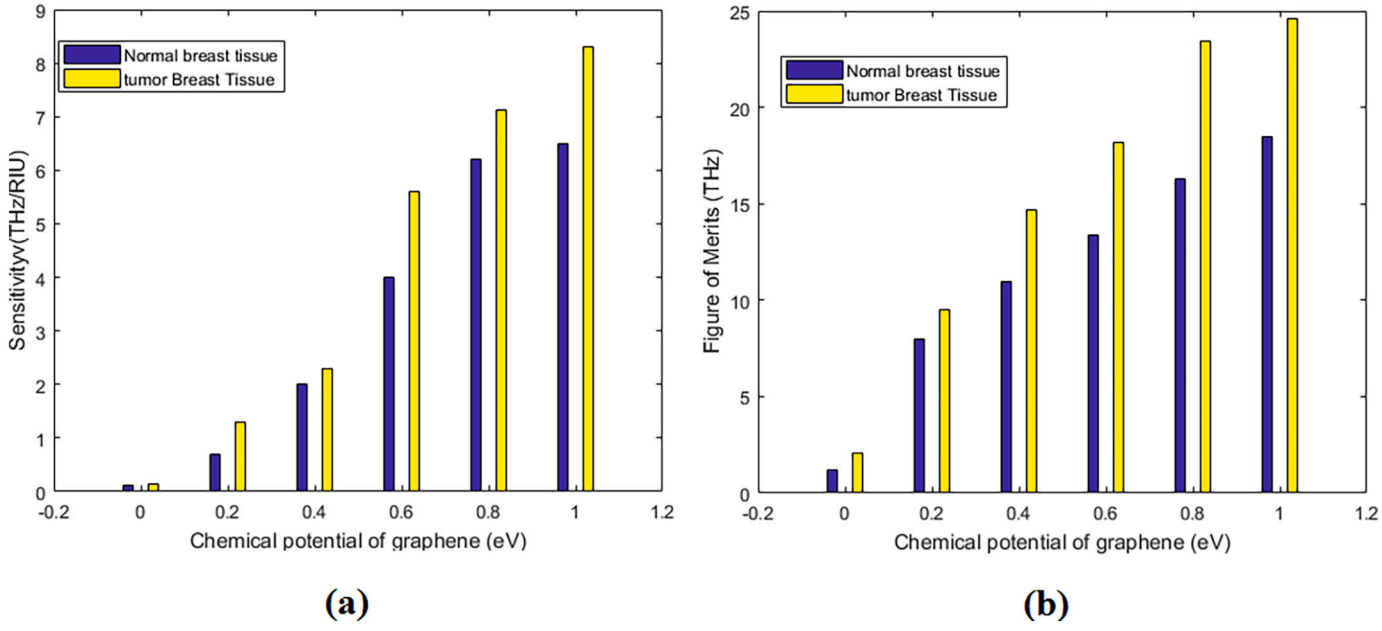

Fig. 20. (a)Sensitivity of the proposed sensor with various values of chemical potential of graphene, (b) Figure of Merits of the proposed sensor with various values of chemical potential of graphene.

conclude that in most cases of the previous work, the proposed antenna has a good property, at sensitivity level and the figure of merits, it can make this antenna very interesting in the future medical sensor.

As we know about the graphene material characteristic conductivity, the chemical potential can be tuned to the resonance frequency, then can improve the gain and VSWR of the antenna. The effect of the change of the graphene chemical potential on the sensitivity, FOM and SAR is presented in Figs. 17 and 20.

However, in these figures, the increase of the chemical potential leads to increased sensitivity, such as 8.4 (THz/RIU) with $\mu_c = 1$ eV. Also an increase in the FOM which reaches 24.9 THz in this chemical potential value. On the other hand, the increase of the chemical potential leads to lower SAR when the chemical potential is greater than 0.6 eV. a peak will be shown 20.2 W/Kg when the chemical potential is 0.1 eV.

6. Conclusion

In this paper, a wideband, terahertz antenna for biosensor devices such as a breast Tumor detection working at terahertz band (4–6 THz) is reported. An improvement is achieved when using a graphene material instead of copper due to high conductivity of the graphene material. Moreover, the antenna performance increases when using SIW technology and the PBG structure at substrate level. The planar antenna structure and its performance makes it a suitable candidate for integration in biosensor devices. The antenna results include CST and HFSS simulations, where simulations are in good agreement, and show the proposed antenna can be a good candidate for biosensor terahertz devices. The simulation results demonstrated that a maximum sensitivity of 8THz/RIU can be achieved for (μ_c =1 eV), operating at a frequency of 4.25 THz.

Declaration of Competing Interest

None.

Acknowledgment

Work was supported in part by project PID2020-113832RB-C22 funded by MCIN/AEI/10.13039/50110001103.

References

[1] H. Kyungho, T.K. Nguyen, I. Park, H. Han, Terahertz Yagi-Uda antenna for high input resistance, J. Infrared Millim. Terahertz Waves 31 (2010) 441–451.
[2] P.R. Smith, D.H. Auston, M.C. Nuss, Subpicosecond photoconducting dipole antennas, IEEE J. Quantum Electron. 24 (2) (Feb. 1988) 255–260.
[3] M. van Exter, C. Fattinger, D. Grischkowsky, Terahertz time-domain spectroscopy of water vapor, Opt. Lett. 14 (1989) 1128–1130.
[4] Q. Wu, F.G. Sun, P. Campbell, X.-C. Zhang, Dynamic range of an electro-optic field sensor and its imaging applications, Appl. Phys. Lett. 68 (1996) 3224–3226.
[5] P.U. Jepson, R.H. Jacobsen, S.R. Keiding, Generation and detection of terahertz pulses from biased semiconductor antennas, J. Opt. Soc. Am. B 13 (1996) 2424–2436.
[6] L. Duvillaret, F. Garet, J.L. Coutaz, A reliable method for extraction of material parameters in terahertz time-domain spectroscopy, IEEE J. Sel. Topics Quantum Electron. 2 (3) (Sep. 1996) 739–746.
[7] D. Mittleman, Sensing with Terahertz Radiation, Springer-Verlag, Heidelberg, Germany, 2002.
[8] A. Hlali, Z. Houaneb, H. Zairi, Effective modeling of magnetized graphene by the wave concept iterative process method using boundary conditions, Progr. Electromagn. Res. C 89 (2019) 121–132.
[9] R. Aloui, Z. Houaneb, H. Zairi, Substrate integrated waveguide circular antenna for terahertz application, Progr. Electromagn. Res. C 96 (2019) 229–242.
[10] F. Sotoodeh, H. Ameri, A novel bandpass waveguide filter structure on SIW technology, Progr. Electromagn. Res. Lett. 2 (2008) 141–148.
[11] P.R. Smith, D.H. Auston, M.C. Nuss, Subpicosecond photoconducting dipole antennas, IEEE J. Quantum Electron. 24 (2) (1988) 255–260.
[12] Eduardo Fontana, Jung-Mu Kim, Ignacio Llamas-Garro, Gustavo Oliveira Cavalcanti, Microfabricated Otto chip device for surface plasmon resonance based optical sensing, Appl. Opt. 54 (November 2015) 9200–9204.
[13] Wanlong Guo, et al., Graphene-based broadband terahertz detector integrated with a square-spiral antenna, Opt. Lett. 43 (8) (2018) 1647–1650.
[14] Young Bin Ji, et al., Terahertz reflectometry imaging for low and high-grade gliomas, Sci. Rep. 6 (2016) 36040.
[15] G.W. Hanson, Dyadic Green's functions and guided surface waves for a surface conductivity model of graphene, J. Appl. Phys. 103 (2008) 064302.
[16] Y.S. Cao, L.J. Jiang, A.E. Ruehli, An equivalent circuit model for graphene-based terahertz antenna using the PEEC method, IEEE Trans. Antennas Prop. 64 (2016) 1385–1393.
[17] Ritesh Kumar, Ž. Kushwahaâ, P. Karuppanan, Enhanced radiation characteristics of graphene-based patch antenna array employing photonic crystals and dielectric grating for THz applications, Int. J. Light Electron Optics 200 (2019), https://doi.org/10.1016/j.ijleo.2019.163422.
[18] Sasmita Dash, Amalendu Patnaik, Material selection for TH z antennas, Wiley Online Library 60 (2018) 1183–1187.
[19] Liaquat Ali, Mahmood Uddin Mohammed, Mahrukh Khan, Abdul Hamid Bin Yousuf, Masud H. Chowdhury, High-quality optical ring resonator-based biosensor for cancer detection, IEEE Sensors J. 20 (2020) 1867–1875.
[20] Afsaneh Keshavarz, Zohreh Vafapour, Sensing avian influenza viruses using terahertz metamaterial reflector, IEEE Sensors J. 19 (2019) 5161–5166.
[21] Seyed Arash Naghdehforushha, Gholamreza Moradi, Plasmonic patch antenna based on graphene with tunable terahertz band communications, Optik (Elsevier) 158 (2018) 617–622.
[22] Jemima Nissiyah George, M. Ganesh Madhan, Phys. E. 94 (2017) 126–131.
[23] G. Liu, M. He, Z. Tian, J. Li, J. Liu, Metamaterial absorber integrated microfluidic terahertz sensors, Appl. Opt. 52 (2013) 5695–5700.
[24] X. Hu, et al., Terahertz surface plasmon sensor for distinguishing gasolines, Laser Photonics Rev. 10 (2016) 962–969.
[25] Y. Zhang, et al., A graphene based tunable terahertz sensor with double Fano resonances, Nanoscale 7 (2015) 12682–12688.
[26] Navin M. George, Thomas Anita Pushpa, Jones Mary, Durable silicon rubber-based miniaturized antenna with concentric circle structure for a medical telemetry application, Progr. Electromagn. Res. M 107 (2022) 155–165.

was born in KEF Village, Tunis in 1990. He received the B.S. and M.S. degrees in National Engineering School of Carthage from the University of Carthage, in 2015 and the Ph.D. degree in electrical engineering (Microwave electronic domain) from University of Carthage, Tunis, in 2021. From 2016 to 2021, he was a Research Assistant at Intelligent Electricity & ICT Research Laboratory, ET TIC Lab. Then he was a Research Assistant at Centre Tecnològic de Telecomunicacions de Catalunya (CTTC).